Available online at www.sciencedirect.com

SciVerse ScienceDirect

Ceramics International 39 (2013) 8385–8392

CERAMICS INTERNATIONAL

www.elsevier.com/locate/ceramint

Citrate–hydrothermal synthesis, structure and electrochemical performance of $La_{0.6}Sr_{0.4}Co_{0.2}Fe_{0.8}O_{3-\delta}$ cathodes for IT-SOFCs

Laurenia M.P. Garcia[a,*], Daniel A. Macedo[b], Graziele L. Souza[c], Fabiana V. Motta[b], Carlos A. Paskocimas[a,b], Rubens M. Nascimento[a,b]

[a]*Postgraduate Program in Mechanical Engineering, Universidade Federal do Rio Grande do Norte, Natal, RN 59072-970, Brazil*
[b]*Postgraduate Program in Materials Science and Engineering, Universidade Federal do Rio Grande do Norte, Natal, RN 59072-970, Brazil*
[c]*Department of Chemical Engineering, Universidade Federal do Rio Grande do Norte, Natal, RN 59072-970, Brazil*

Received 26 February 2013; received in revised form 2 March 2013; accepted 5 April 2013
Available online 15 April 2013

Abstract

$La_{0.6}Sr_{0.4}Co_{0.2}Fe_{0.8}O_{3-\delta}$ (LSCF) powders were synthesized by a combination of citrate and hydrothermal methods. The thermal decomposition behavior of the as-prepared powder was carried out by simultaneous thermogravimetry–differential thermal analysis. The calcined powders were investigated by X-ray diffraction (XRD), scanning electron microscopy (SEM) and particle size distribution (PSD). Screen-printed LSCF/CGO/LSCF symmetrical cells were sintered between 1150 and 1200 °C and studied by impedance spectroscopy in order to assess the cathode kinetics for the oxygen reduction reaction. Rietveld refinement of XRD data showed the formation of a single perovskite LSCF phase with crystallite size of 53 nm at 900 °C. The best area specific resistance (ASR) value, measured in static air, was found to be 0.34 Ω cm^2 at 750 °C, demonstrating that the novel citrate–hydrothermal method is an effective way to prepare cathode materials for SOFC. Cathode performance can be further enhanced by additional surface modification through impregnation with Pr-containing solution, reaching 0.17 Ω cm^2 at 750 °C. Furthermore, the activation energy of the PrO_x-impregnated cathode is 83.4 kJ/mol, i.e., much lower than 123.8 kJ/mol, the best value determined for PrO_x-free cathodes.

Keywords: Citrate–hydrothermal method; LSCF; Microstructure; Praseodymium oxide; Impedance spectroscopy

1. Introduction

Fuel cells are highly efficient power generation devices which convert chemical energy from fuels like hydrogen and ethanol directly into electric power. It takes place in a silent and environmentally friendly way. These electrochemical devices are promising alternatives to traditional mobile and stationary power sources, such as internal combustion engines and coal burning power plants. Among the various types of fuel cells, solid oxide fuel cells (SOFCs) have advantages such as high energy conversion efficiency and excellent fuel flexibility due to their high operating temperature compared to other types of fuel cells. A typical SOFC single cell consists of three basic components: two porous electrodes (anode and cathode) and a solid electrolyte. Each one of these components must fulfill specific performance requirements such as microstructural stability during preparation and operation; chemical and physical compatibility, i.e. similar thermal expansion coefficients; adequate porosity and catalytic activity to achieve the highest performance [1–3].

SOFCs have attracted significant attention in the last three decades due to their high efficiency, fuel flexibility and environmental advantages [4,5]. However, typical SOFCs operate at 1000 °C. These elevated operation temperatures introduce a series of difficulties such as sintering of electrodes and high reactivity between cell components. For these reasons, there is a considerable research interest in reducing the operation temperature of these devices down to the range from 500 to 800 °C, which characterizes intermediate temperature of solid oxide fuel cells (IT-SOFCs). This would imply the use of inexpensive metallic materials, rapid start-up and shut-down, minimization of thermal degradation and

*Corresponding author. Tel.: +55 84 3215 3826; fax: +55 84 3215 3183.
E-mail address: lauengmat@hotmail.com (L.M.P. Garcia).

0272-8842/$ - see front matter © 2013 Elsevier Ltd and Techna Group S.r.l. All rights reserved.
http://dx.doi.org/10.1016/j.ceramint.2013.04.019

reactions between cell components, and longer operational lifetime [6,7].

On the other hand, lowering operation temperature reduces the overall electrochemical performance due to increased ohmic losses and electrode polarization losses associated with thermally activated processes of both ionic transport and electrode reactions. In special, the electrochemical activity of the cathode dramatically deteriorates with decreasing temperature for typical perovskite-type manganite-based materials such as LSM ($La_{1-x}Sr_xMnO_{3-\delta}$). In addition, with regard to anode-supported SOFCs, the most promising solid oxide fuel cell configuration, cathode polarization resistance (or area specific resistance, ASR) is the major contribution to the total cell loss and for intermediate temperature operation, this becomes more serious. Due to the higher activation energy and lower reaction kinetics for oxygen reduction in the cathode compared with those of fuel oxidation in the anode, the polarization loss from the air electrode (cathode) limits the overall cell performance [8,9]. Therefore, the development of new cathode materials and microstructures with high electrocatalytic activity for oxygen reduction becomes a critical issue for maintaining cell performance below 800 °C.

To that end, recent studies on the synthesis of SOFC cathodes have focused on lanthanum strontium cobaltite ferrites ($La_{1-y}Sr_yCo_{1-x}Fe_xO_{3-\delta}$ -LSCF), which show superior electrical properties compared to traditional LSM cathodes. LSMs are poor ionic conductors and the electrochemical reactions are limited to the region close to triple-phase boundaries (TPBs). On the other hand, LSCF is a mixed electronic/ionic conductor (MEIC) with appreciable ionic conductivity in which the exchange of oxygen ions takes place at the electrode surface with oxygen diffusion through the mixed conductor [10–12].

Among the extensive number of chemical synthesis routes available for the preparation of LSCF powders, the modified combined complexing method [12], acetate and HMTA methods [13], and combustion synthesis [14] have been successfully used. Alternative synthesis methods using microwave technology have also been implemented in an attempt to minimize energy consumption and total powder production time [11,15]. Regarding wet-chemical methods, the hydrothermal method has emerged as an attracting technique for the production of high-purity materials. This is because the hydrothermal crystallization is a self-cleansing process, during which crystallites tend to reject impurities present in the growth environment [16]. It is noteworthy that the hydrothermal source is an inexpensive, reproducible, and environment-friendly method. However, in some cases, the reaction takes place in a single step, while sometimes further annealing is necessary to obtain material free of secondary phases. For doped materials, the hydrothermal method can often be combined with others [17,18].

A promising method for improving the performance of cathodes is treatment with electrocatalytically active agents such as Ag, Pd, Pt, samarium/gadolinium doped ceria, and praseodymia [19–23]. Such impregnation (or infiltration) process with catalytically and/or electrochemically active nanoparticles onto a porous supporting structure can enhance the electrocatalytic activity by increasing the number of reactive sites available for the oxygen reduction reaction on perovskite-type cathodes such as LSM and LSCF. For example, the area specific resistance of a LSCF cathode decreased from 0.22 Ω cm^2 to 0.1 Ω cm^2, at 750 °C, after impregnation with 1.2 mg cm^{-2} Pd [21].

Continuing our research on electrode materials for IT-SOFCs [15,24,25], the present work is focused on the preparation of $La_{0.6}Sr_{0.4}Co_{0.2}Fe_{0.8}O_{3-\delta}$ powders by a novel citrate–hydrothermal method. To the best of our knowledge, such a combination of chemical routes to obtain LSCF has not yet been reported. Scanning electron microscopy and impedance spectroscopy were used to assess the effects of the electrode sintering condition on the cathode performance. The cathode with better electrochemical performance was impregnated with praseodymia (PrO_x) and its electrocatalytic activity for the oxygen reduction reaction was compared with samples without impregnation.

2. Experimental procedure

2.1. Citrate–hydrothermal synthesis of LSCF powders

Lanthanum strontium cobaltite ferrite (LSCF) powders were obtained, for the first time, by a combination of citrate and hydrothermal methods. The nominal composition of $La_{0.6}Sr_{0.4}Co_{0.2}Fe_{0.8}O_{3-\delta}$ (LSCF6428) was prepared using metal nitrates (> 99.0% Sigma-Aldrich) and citric acid (> 99.0% VETEC, Brazil) as starting materials. The LSCF composition was selected because its desirable properties for IT-SOFC cathode applications are well established in literature [26]. Stoichiometric amounts of nitrates were dissolved in distilled water under magnetic stirring and heating at 60 °C. After complete dissolution of salts, citric acid was added at molar ratio of 1:2 (metal:citric acid). Under these conditions, a clear yellow solution of pH = 3 was obtained after about 1 h. The as-prepared solution derived from the citrate method was transferred to the hydrothermal reactor, where it was submitted to hydrothermal treatment at 150 °C for 3 h. The resulting powder was dried at 75 °C for 30 min and ground in an agate mortar.

2.2. Characterization of LSCF powders

As-prepared LSCF powder was characterized by simultaneous thermogravimetry–differential thermal analysis and calcined between 700 and 900 °C for 4 h. The thermal decomposition behavior of the precursor powder was made using a TG/DTA simultaneous analyzer model TG/DTA-60 Shimadzu, from room temperature to 1000 °C and air flow of 50 cm^3/min. The calcined powders were characterized by X-ray diffraction (XRD) using a Shimadzu XRD-7000 diffractometer (CuK_α radiation, with 40 kV and 40 mA). The diffraction patterns were obtained within the angular range of $20 \leq 2\theta \leq 80^\circ$ in the step-scanning mode (0.02°/step, 2 s/step). Rietveld refinement of the XRD data was made using the Maud software, which was developed to analyze diffraction

spectra and obtain crystal structures, quantity and microstructure of phases along with texture and residual stresses. It applied the RITA/RISTA method as developed by Ferrari and Lutterotti [27]. Particle size distribution was obtained by laser scattering (Cilas 1064 granulometer) with ultrasound treatment for 90 s in distilled water. The morphological analysis of particles was performed with a Philips XL-30 scanning electron microscope. Based on XRD results, the LSCF powder calcined at 900 °C was highly energy milled in a planetary milling at 500 rpm for 3 h and then ball milled under 50 rpm for 1 h. The particle size distribution **(PSD)** of the milled powder was re-measured. Finally, the specific surface area (BET method) of the milled powder was obtained on a Flow Prep 060 Micromeritrics apparatus using nitrogen adsorbate.

2.3. Preparation and characterization of symmetrical cells

The powder calcined at 900 °C was mixed with a commercial organic vehicle (Quimiceram, Portugal) and the resulting slurry was screen-printed on both sides of dense $Ce_{0.9}Gd_{0.1}O_{1.95}$ (CGO) pellets, cold isostatically pressed under 200 MPa and sintered at 1550 °C for 4 h. The screen-printed cathodes were sintered at 1150 °C for 4 h and 1200 °C with dwell times from 1 to 2 h, resulting in a LSCF/CGO/LSCF symmetrical cell configuration used for electrochemical measurements. After electrochemical tests, a selected cathode was surfaced modified by impregnation with $Pr(NO_3)_3 \cdot 6H_2O$ solution in ethanol (0.35 mol L^{-1}), followed by annealing at 800 °C for 1 h; then electrochemical performance was re-measured.

The electrode area was 0.2 cm^2 after sintering. Two Pt meshes were attached to the cathodes as current collectors for electrochemical measurements. ASR values were determined from impedance spectroscopy at open circuit voltage with temperature ranging from 650 to 800 °C in static air. The amplitude of the AC signal was 100 mV and the frequency ranged from 20 Hz to 1 MHz. Smaller amplitudes (30, 50 mV) were tested and gave responses of similar magnitude but of poorer resolution. ASR was determined by the difference between high and low frequency intercepts in the impedance axis. Impedance data were corrected for electrode area and divided by two (symmetric cell) to obtain the ASR value of each cathode. Although 1 Hz or lower is usually required to obtain a complete electrode response, the cathodes produced herein had their two electrode processes (diffusion and charge-transfer) successfully revealed using lower frequency limit of 20 Hz. The possibility of using this frequency range, without information loss of the electrochemical performance, has also been reported [28]. A third impedance arc in very low frequencies is not observed if the partial oxygen pressure is equal to or higher than 0.21 atm, as in the case of the present study. Further evidence to corroborate the choice of frequency range made in this study can also be found in another related work [29]. Even though a frequency range from 0.01 Hz to 1 MHz was used to evaluate the effect of ZnO doping on the performance of cobaltite-based cathodes, the similarity between the impedance spectra reported in that work and those reported herein is clearly visible. This confirms that the lower frequency limit of 20 Hz does not imply any limitation of the electrode response. The surface and cross-section of cathodes were inspected using scanning electron microscopy (Tabletop Microscope, Hitachi, TM-3000). Porosity was estimated by SEM image analysis (using ImageJ) of the surface morphology.

3. Results and discussion

3.1. Characterization of powders

3.1.1. Thermal analysis

Fig. 1 shows TGA and DTA curves for the LSCF precursor powder as-prepared by the citrate–hydrothermal method. Thermal decomposition takes place in four steps between 30 and 1000 °C. The two first decomposition steps (from room temperature to around 364 °C) can be assigned to the loss of adsorbed water and decomposition of metal-citrate complexes. The third step of weight loss, characterized by nitrate decomposition, takes place up to 500 °C. The total decomposition of organ residues occurs up to around 600 °C (fourth step). Finally, the material begins to stabilize at approximately 700 °C, followed by a small weight gain of 0.9% due to oxidation in the temperature range of 736–762 °C. The thermogravimetric analysis is corroborated by the DTA curve, in which the two first peaks are related to endothermic processes and the other two are attributed to exothermic events.

3.1.2. XRD analysis

Fig. 2 shows X-ray diffraction patterns of LSCF powders calcined between 700 and 900 °C. The profiles presented characteristic peaks of the perovskite LSCF phase together with small amount of secondary phases (La_2O_3, $LaSrCoO_4$ and $La(OH)_3$) for powders calcined below 900 °C. The hydration of La_2O_3 at high temperatures led to the appearance of the La $(OH)_3$ phase, in accordance with results previously reported by Ghosh et al. [30]. The complete formation of a single perovskite LSCF phase can be achieved at 900 °C. It could be observed that the LSCF diffraction peaks become sharper and more intense with increasing calcination temperature,

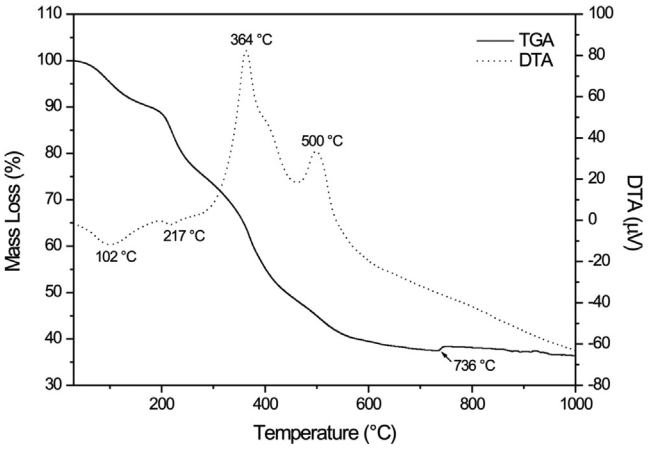

Fig. 1. TGA and DTA curves of the LSCF precursor powder.

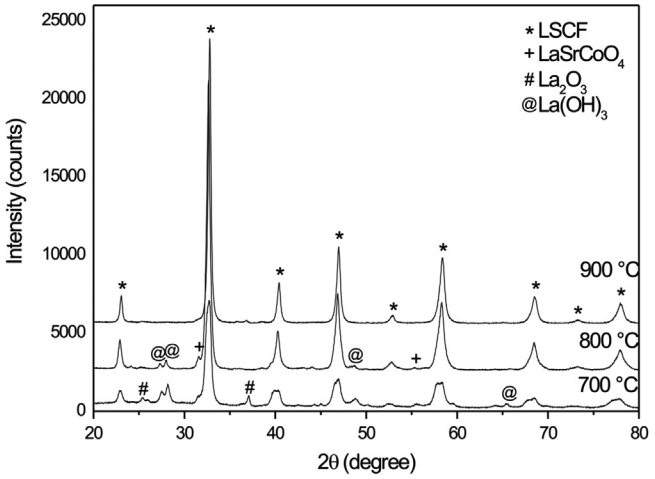

Fig. 2. XRD patterns of the LSCF powders calcined between 700 and 900 °C.

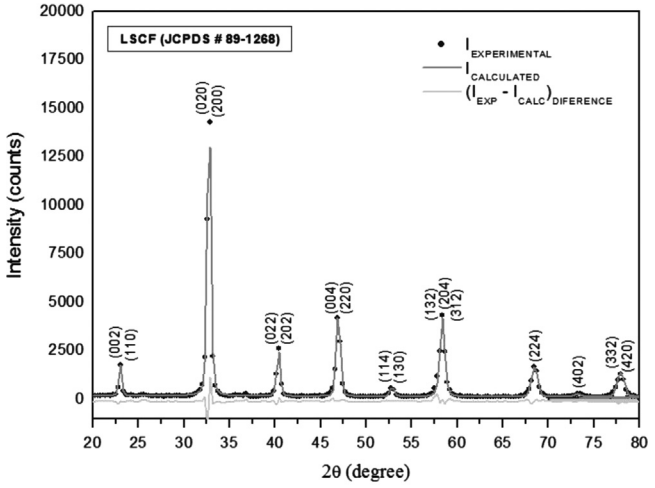

Fig. 3. XRD patterns (experimental, calculated and difference) from the Rietveld refinement of the LSCF powder calcined at 900 °C.

which suggests a gradual growth in the crystallite size and an increase in phase crystallinity.

Fig. 3 shows the XRD patterns, including the one calculated from the Rietveld refinement for the LSCF powder calcined at 900 °C. All the diffraction peaks were indexed according to the rhombohedral symmetry with Pbnm space group, i.e. there are no obvious peaks from phases other than $La_{0.6}Sr_{0.4}Co_{0.2}Fe_{0.8}O_3$ (JCPDS 89-1268) according to the detection limit of this technique. The lattice parameters obtained are in agreement with reported parameters ($a=5.4919$ Å; $b=5.4920$ Å; and $c=7.7691$ Å; JCPDS 89-1268) and the calculated crystallite size (53 nm) is in accordance with those reported by Zhou et al. [31] for LSCF powders prepared by different synthesis methods. The χ^2 value (goodness-of-fit) obtained, equal to 2.9, indicates a good quality fit.

3.1.3. Particle size distribution and morphology

Fig. 4 shows the PSD curves and micrographs for the LSCF powder calcined at 900 °C, before and after grinding in mills of high energy (500 rpm for 3 h) and balls (50 rpm for 1 h). The average particle/agglomerate size at 50% (d_{50}) was reduced from 30.34 to 0.975 μm after milling processes. Such significant reduction in particle size is suitable for preparing cathode–electrode slurry for film deposition by screen-printing. SEM images of powders before and after milling processes are illustrated in Fig. 4b and d, which provides a direct visual comparison of the agglomerate morphologies. Fig. 4b clearly shows that the as-calcined powder exhibits morphology with strong presence of micrometric agglomerates, while powder obtained following grinding showed clusters less than 5 μm, in agreement with the correspondent PSD curve.

The milled LSCF powder had its specific surface area measured using the BET analysis and was examined using higher SEM magnification. A cathode powder with surface area of 5.2 m^2/g and consisting of agglomerates with almost-spherical nano-sized particles ($<$ 100 nm) can easly be seen in Fig. 5. This is in agreement with the crystallite size obtained from XRD analysis, suggesting that the majority of particles are nanostructured. The surface area obtained is coherent in magnitude with those reported for powders prepared under similar calcining conditions [13,32,33].

3.2. Characterization of symmetrical cells

3.2.1. Microstructure

Since the microstructure of sintered cathodes is one of the most important factors to influence electrochemical performance, surface morphologies and a typical cross-section image of symmetrical cells prepared from the LSCF powder calcined at 900 °C and sintered at different temperatures are shown in Fig. 6. It could be observed (Fig. 6(a) that LSCF cathode prepared at 1150 °C exhibits a highly porous microstructure (57% porosity), which may be detrimental for the mechanical strength, electrical conductivity and permeation of the oxidant fuel in the cathode. For cathodes sintered at 1200 °C (Fig. 6b–c), a progressive reduction in porosity with increasing sintering dwell time is clearly visible. By SEM image analysis of the surface morphologies, electrodes with 38% and 32% porosity were obtained for dwell times of 1 and 2 h, respectively.

A uniform, porous and well-sintered structure with sub-micron grains, beneficial for gas transportation and formation of the electronic conducting network within the cathode was achieved after sintering at 1200 °C/2 h (Fig. 6c). Further reduction in electrode porosity is expected to reduce cathode electrochemical performance due to mass transport limitations. Fig. 6d shows a representative SEM image of the cross-section for the symmetrical cell sintered at 1200 °C/1 h. It could be observed that the porous and crack-free LSCF cathode and dense CGO substrate adhered well to each other under the processing condition used to produce the symmetric cell. The cathode thickness is about 30–40 μm and no delamination occurred at the cathode/electrolyte interface. By taking into account that theoretical and experimental considerations suggest that the electrochemically active region typically extends 10–20 μm from the electrolyte into the electrode [34,35],

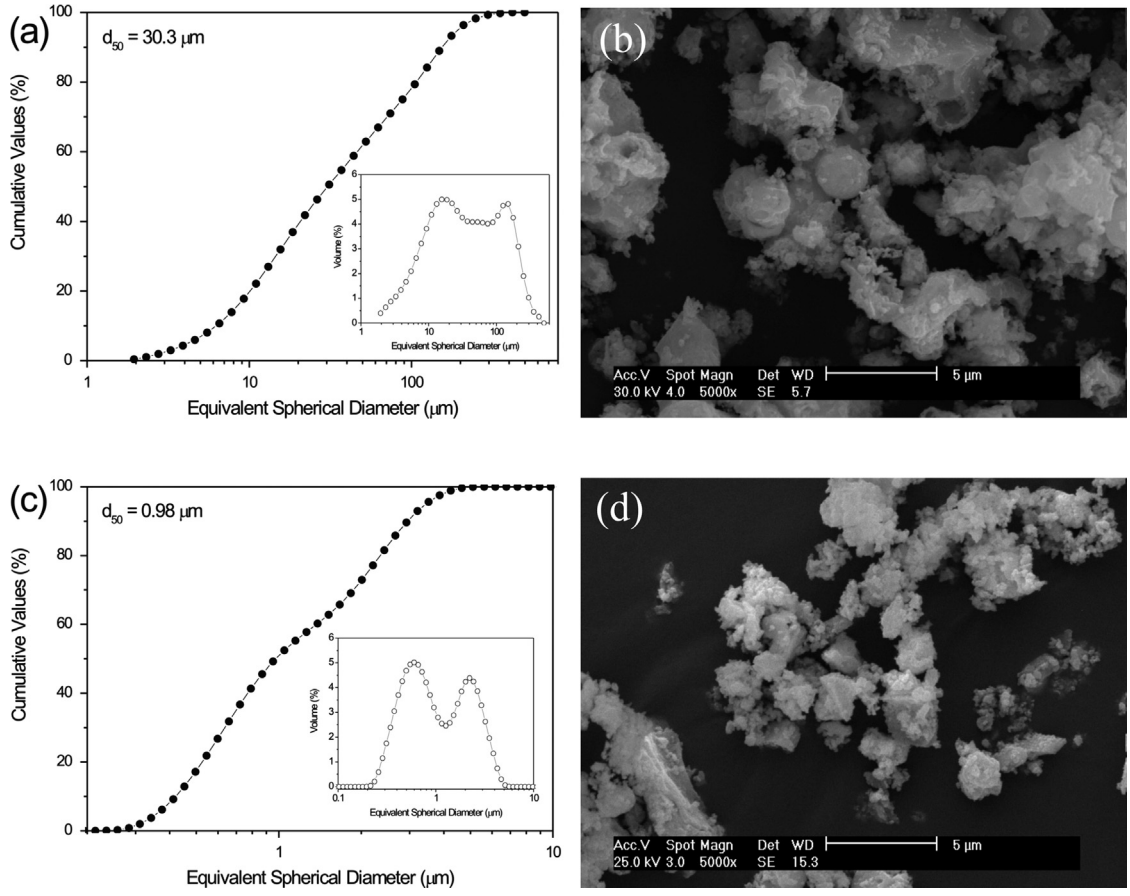

Fig. 4. Particle size distribution curves and SEM images of the powder calcined at 900 °C, before (a and b) and after (c and d) milling.

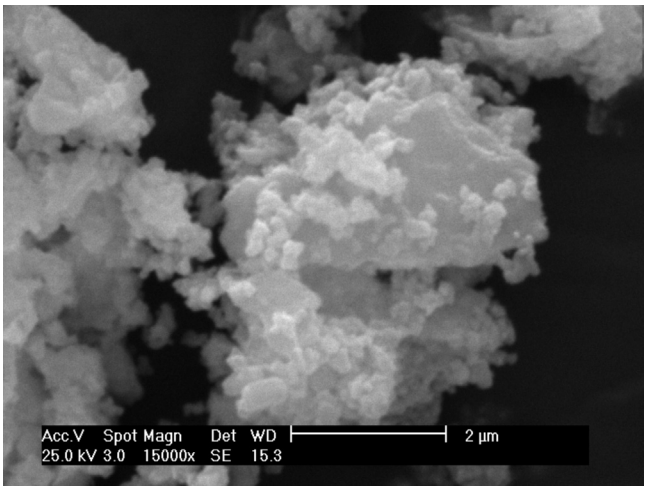

Fig. 5. Particle size and morphology of the milled powder.

cathodes obtained herein were optimally screen-printed using LSCF powder synthesized by the citrate–hydrothermal method.

It was well established that cathode performance can be further enhanced by additional surface modification through impregnation with precursor solutions containing electrocatalytic species [19,36]. In this study, the effect of impregnation with $Pr(NO_3)_3 \cdot 6H_2O$ solution in ethanol (0.35 mol L^{-1}) on the electrochemical performance of the cathode sintered at 1200 °C/2 h was investigated by impedance spectroscopy. Fig. 7 shows a typical SEM image and the Pr distribution for the porous PrO_x-impregnated LSCF cathode. As can be seen, after impregnation the cathode microstructure is characterized by the formation of uniformly distributed praseodymium oxide particles on the surface of LSCF grains.

3.2.2. Electrochemical performance

The electrochemical performance of screen-printed cathodes for the O_2 reduction reaction (ORR) was evaluated by impedance spectroscopy at different temperatures from 650 to 800 °C. Fig. 8 shows typical impedance spectra of the ORR, measured at 800 °C in static air, on LSCF cathodes sintered at 1150 and 1200 °C. All spectra shown in this study were fitted with the equivalent circuit $LR_1(R_2CPE_1)^{HF}(R_3CPE_2)^{LF}$, using nonlinear least squares fitting the Z-view program. The presence of two arcs in the impedance spectra suggests that at least two different electrode processes limited the ORR. In the circuit mentioned above, L is an inductance element and R_1 is the electrolyte contribution including the electrolyte resistance, as well as the resistance of leads in series with two electrode elements consisting of resistances (R_2 and R_3) in parallel with constant phase elements (CPE_1 and CPE_2). Each CPE has a CPE-T, which is related to the relaxation capacitance; and a CPE-P, which reflects the displacement of the arc center from the real axis.

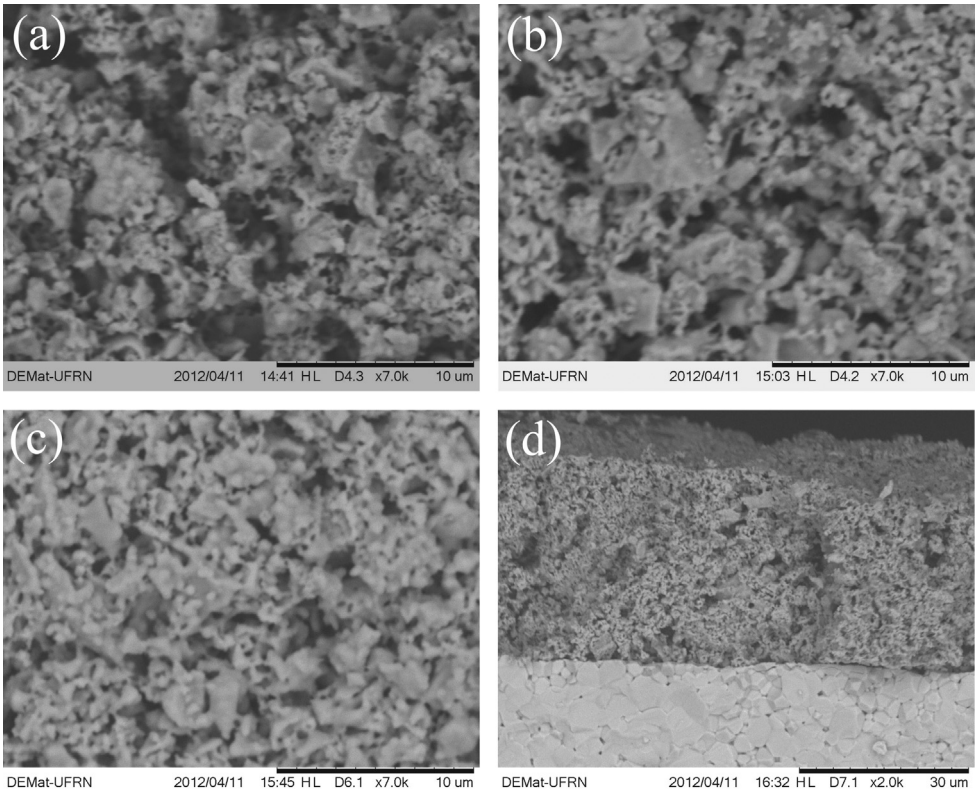

Fig. 6. SEM images of the surface of cathodes sintered at (a) 1150 °C/4 h, (b) 1200 °C/1 h, and (c) 1200 °C/2 h, and a typical cross-section image of the symmetrical cell sintered at 1200 °C/1 h.

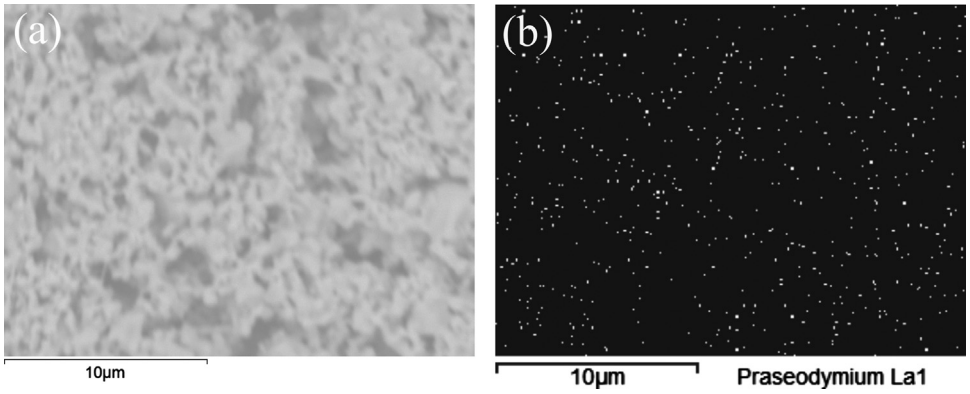

Fig. 7. SEM image (a) and Pr distribution (b) of the PrO_x-impregnated LSCF cathode.

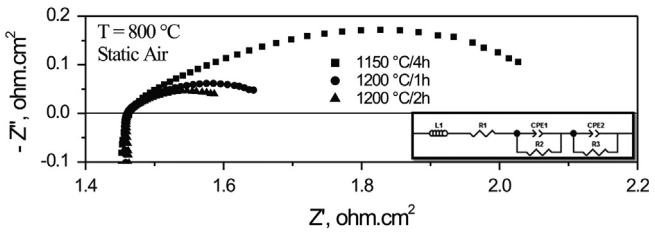

Fig. 8. Impedance spectra of different LSCF cathodes measured at 800 °C in static air and the equivalent circuit used to fit the impedance data.

The low frequency arc can be attributed to diffusion processes, which include oxygen adsorption–desorption, oxygen diffusion at the gas–film interface and surface diffusion of intermediate oxygen species. The high frequency arc is probably associated with charge–transfer processes, which include oxide ion diffusion in the cathode bulk and incorporation of oxygen ions from three-phase boundaries [37,38]. From impedance spectra, the area specific resistance (ASR) was directly obtained from the difference between high- and low-frequency intercepts on the real axis of the fitted impedance plots. The overall ASR, which characterizes the electrochemical performance of each composite cathode, corresponds to the sum of the oxygen ions transport and charge transfer processes ($ASR=R_2+R_3$). In order to assist the comparative electrochemical performance analysis, the electrolyte ohmic resistance was subtracted in Fig. 8. Impedance spectroscopy data for both

symmetric cells (LSCF/CGO/LSCF) were adequately fitted to the aforementioned equivalent circuit.

As can be observed from Fig. 8, there was a significant reduction in the impedance for oxygen reduction on the LSCF cathode sintered at 1200 °C/2 h, indicating a considerable enhancement of its electrochemical activity compared to those of more porous cathodes. Manipulating the cathode microstructure by changing the sintering conditions allowed reducing the overall ASR from 0.68 Ω cm^2 (sintering at 1150 °C/4 h) to 0.25 Ω cm^2 (sintering at 1200 °C/1 h) and further to 0.18 Ω cm^2 (sintering at 1200 °C/2 h) at the highest operation temperature tested, providing more than 70% improvement of the cathode electrochemical performance by microstructural design. At 650 °C, ASR was 9.67 Ω cm^2 for the ORR on the cathode sintered at 1150 °C/4 h, lowering to 4.29 and 1.67 Ω. cm^2 on electrodes prepared at 1200 °C with dwell times of 1 and 2 h, respectively. The improved electrochemical activity of the cathode prepared at the highest dwell time at 1200 °C is mainly attributed to its microstructural optimization, especially with regards to proper porosity for oxygen permeation.

Fig. 9 shows the activation energies for LSCF cathodes sintered between 1150 and 1200 °C. The first think to note is that ASR is temperature-activated during oxygen reduction. The temperature-dependence for all cathodes was nearly linear, and activation energy (Ea) values calculated from the slope of linear fit were 146.8 kJ/mol, 157.8 kJ/mol and 123.8 kJ/mol. The activation energy for ORR on the electrode sintered at 1200 °C/2 h is similar to that reported for the $Ba_{0.5}Sr_{0.5}Co_{0.8}Fe_{0.2}O_{3-\delta}$ (BSCF) cathode prepared by electrostatic slurry spray deposition [39].

Fig. 10 shows the temperature-dependence of ASR for cathodes sintered at 1200 °C, with and without PrO_x impregnation. It could be observed that the surface modification drastically increases the electrochemical activity of the ORR, especially at reduced temperatures. For instance, at 700 °C, the ASR is decreased by more than two times, from 0.75 down to 0.31 Ω cm^2, as a result of the impregnation with praseodymia. At 750 °C, ASR was 0.52 Ω cm^2 for PrO_x-free cathode sintered at 1200 °C/1 h, decreasing to 0.17 Ω cm^2 for PrO_x-impregnated cathode sintered at 1200 °C/2 h. ASR values for PrO_x-impregnated cathode are similar to those reported in literature [21,39]. Impregnation of PrO_x particles into porous LSCF cathode has also a significant effect on the activation energy, which was reduced from 123.8–157.8 kJ/mol to 83.4 kJ/mol, as can be seen in Fig. 10. Such enhancement in cathodic performance may be attributed to the combination of two phenomena: enlargement of the electrode surface area and improvement of the electrode transport properties due to significant mixed conductivity of the praseodymium oxide, as previously reported by Tikhonovich et al. [19] and Kharton et al. [36]. Further investigation is required to assess the electrochemical performance of these cathodes as a function of the partial oxygen pressure.

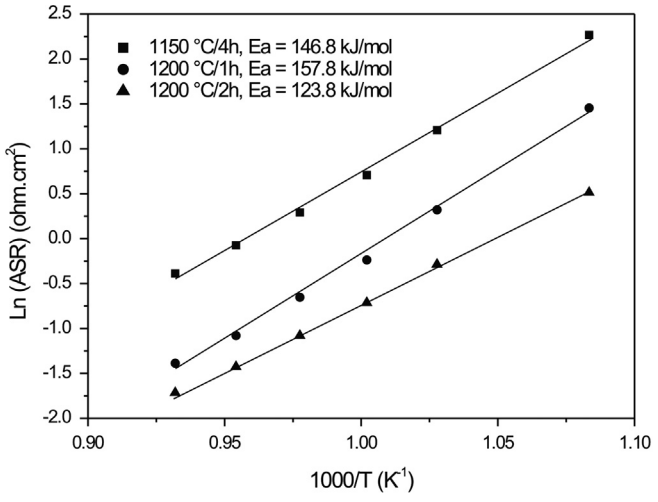

Fig. 9. Activation energies for cathodes prepared at different sintering conditions.

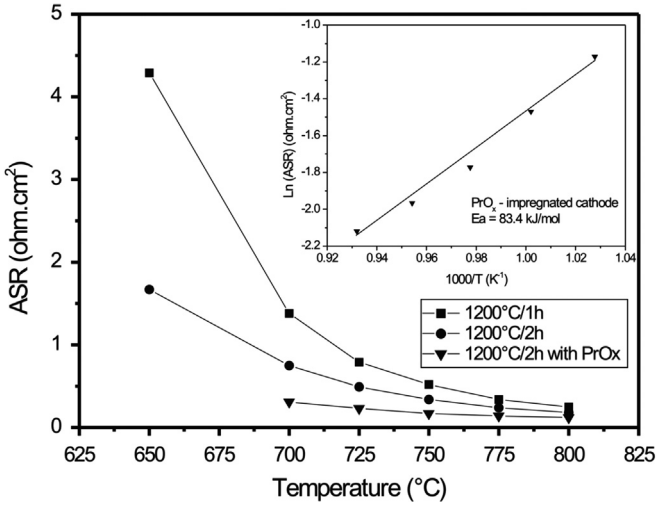

Fig. 10. Temperature dependence of the ASR for cathodes sintered at 1200 °C. The inset shows the activation energy for the PrO_x-impregnated cathode.

4. Conclusion

LSCF powders have been synthesized by the combination of citrate and hydrothermal methods and assessed for possible use as porous cathodes in SOFCs. Even though thermal analyses indicate phase crystallization below 800 °C, the complete formation of pure LSCF perovskite-type structure with nano-sized particles was achieved at 900 °C. Further reduction of agglomerate/particle size by milling processes resulted in a sub-micron powder, suitable for preparing slurry for deposition of porous and crack-free LSCF cathodes by screen-printing. There was a sensitive dependence of both microstructure and electrochemical performance with regard to the cathode sintering condition. At operation temperature of 750 °C, ASR was reduced from 0.52 to 0.34 Ω cm^2 by increasing the sintering dwell time at 1200 °C. Electrocatalytic activity was further improved through impregnation with praseodymia, reaching 0.17 Ω cm^2 at 750 °C. Furthermore, the activation energy of the PrO_x-impregnated cathode is 83.4 kJ/mol, much lower than those found for PrO_x-free cathodes. These results indicated that the citrate–hydrothermal method used in this

study is an innovative alternative for the production of a promising functional material for SOFC cathodes.

Acknowledgments

The authors acknowledge PPGEM-UFRN, PPGCEM-UFRN, National Agency of Petroleum, Natural Gas and Biofuels (ANP-PRH 14), and CAPES for the financial support. The electrochemical characterization was performed at the Department of Materials & Ceramic Engineering of the University of Aveiro (Portugal).

References

[1] N.Q. Minh, T. Takahashi, Science and technology of ceramic fuel cell, Elsevier, 1995.
[2] S.C. Singhal, Advances in solid oxide fuel cell technology, Solid State Ionics 135 (2000) 305–313.
[3] H. Yokokawa, N. Sakai, T. Horita, K. Yamaji, Recent developments in solid oxide, Fuel Cells 1 (2001) 117.
[4] N.Q. Minh, Solid oxide fuel cell technology—features and applications, Solid State Ionics 174 (2004) 271–277.
[5] J. Molenda, K. Swierczek, W. Zajac, Functional materials for the IT-SOFC, Journal of Power Sources 173 (2007) 657–670.
[6] N.P. Brandon, S. Skinner, B.C.H. Steele, Recent advances in materials for full cells, Annual Review of Materials Research 33 (2003) 183–213.
[7] A. Tarancón, Strategies for lowering solid oxide fuel cells operating temperature, Energies 2 (2009) 1130–1150.
[8] E. Ivers-Tiffee, A. Weber, D. Herbstritt, Materials and technologies for SOFC-components, Journal of the European Ceramic Society 21 (2001) 1805–1811.
[9] J. Fleig, Solid Oxide Fuel Cell Cathodes: polarization mechanisms and modeling of the electrochemical performance, Annual Review of Materials Research 33 (2003) 361–382.
[10] M.M. Natile, $La_{0.6}Sr_{0.4}Co_{1-y}Fe_yO_{3-\delta}$ perovskites: influence of the Co/Fe atomic ratio on properties and catalytic activity toward alcohol steam-reforming, Chemistry of Materials 20 (2008) 2314–2327.
[11] S. Liu, X. Qian, J. Xiao, Synthesis and characterization of $La_{0.8}Sr_{0.2}Co_{0.5}Fe_{0.5}O_{3-\delta}$ nanopowders by microwave assisted sol–gel route, Journal of Sol–Gel Science and Technology 44 (2007) 187–193.
[12] J. Shao, Y. Tao, J. Wang, C. Xu, W.G. Wang, Investigation of precursors in the preparation of nanostructured $La_{0.6}Sr_{0.4}Co_{0.2}Fe_{0.8}O_{3-\delta}$ via a modified combined complexing method, Journal of Alloys and Compounds 484 (2009) 263–267.
[13] L. Baqué, A. Caneiro, M.S. Moreno, A. Serquis, High performance nanostructured IT-SOFC cathodes prepared by novel chemical method, Electrochemistry Communications 10 (2008) 1905–1908.
[14] L. Conceição, A.M. Silva, N.F.P. Ribeiro, M.M.V.M. Souza, Combustion synthesis of $La_{0.7}Sr_{0.3}Co_{0.5}Fe_{0.5}O_3$ (LSCF) porous materials for application as cathode in IT-SOFC, Materials Research Bulletin 46 (2011) 308–314.
[15] M.R. Cesário, D.A. Macedo, A.E. Martinelli, R.M. Nascimento, B.S. Barros, D.M.A. Melo, Synthesis, structure and electrochemical performance of cobaltite-based composite cathodes for IT-SOFC, Crystal Research and Technology 47 (2012) 723–730.
[16] W.L. Suchanek, R.E. Riman, Hydrothermal synthesis of advanced ceramic powders, Advanced Sciences and Technologies 45 (2006) 184–193.
[17] W. Junxi, Y. Youwei, M. Chunyan, T. Guoyi, Citrate-mediated hydrothermal route to synthesis a large-scale Y2O3:Eu3+ hexangular prism, Journal of Rare Earths, 25, 115–119.
[18] C. Bernard, C. Laberty, F. Ansart, B. Durand, Hydrothermal synthesis of $La_{1-x}Sr_xMnO_{3+\delta}$ manganites, Annales de Chimie Science des Matériaux 28 (2003) 85–96.
[19] V.N. Tikhonovich, V.V. Kharton, E.N. Naumovich, A.A. Savitsky, Surface modification of La(Sr)MnO_3 electrodes, Solid State Ionics 106 (1998) 197–206.
[20] Y. Sakito, A. Hirano, N. Imanishi, Y. Takeda, O. Yamamoto, Y. Liu, Silver infiltrated $La_{0.6}Sr_{0.4}Co_{0.2}Fe_{0.8}O_3$ cathodes for intermediate temperature solid oxide fuel cells, Journal of Power Sources 182 (2008) 476–481.
[21] J. Chen, F. Liang, B. Chi, J. Pu, S.P. Jiang, L. Jian, Palladium and ceria infiltrated $La_{0.8}Sr_{0.2}Co_{0.5}Fe_{0.5}O_{3-\delta}$ cathodes of solid oxide fuel cells, Journal of Power Sources 194 (2009) 275–280.
[22] K. Sasaki, J. Tamura, H. Hosoda, T.N. Lan, K. Yasumoto, M. Dokiya, Pt-perovskite cermet cathode for reduced-temperature SOFCs, Solid State Ionics 148 (2002) 551–555.
[23] L. Nie, M. Liu, Y. Zhang, M. Liu, $La_{0.6}Sr_{0.4}Co_{0.2}Fe_{0.8}O_{3-\delta}$ cathodes infiltrated with samarium-doped cerium oxide for solid oxide fuel cells, Journal of Power Sources 195 (2010) 4704–4708.
[24] B. Cela, D.A. Macedo, G.L. Souza, A.E. Martinelli, R.M. Nascimento, C.A. Paskocimas, Strontium-doped lanthanum manganite synthesis for solid oxide fuel cells cathode, Journal of New Materials for Electrochemical Systems 12 (2009) 109.
[25] D.A. Macedo, M.R. Cesário, B. Cela, D.M.A. Melo, C.A. Paskocimas, A.E. Martinelli, R.M. Nascimento, Influence of polymerizing agent on structure and spectroscopic properties of nano-crystalline $La_{0.8}Sr_{0.2}MnO_3$ powders, Crystal Research and Technology 45 (2010) 1166.
[26] A. Esquirol, N.P. Brandon, J.A. Kilner, M. Mogensen, Electrochemical characterization of $La_{0.6}Sr_{0.4}Co_{0.2}Fe_{0.8}O_3$ cathodes for intermediate-temperature SOFCs, Journal of the Electrochemical Society 151 (2004) A1847–A1855.
[27] M. Ferrari, L. Lutterotti, Method for the simultaneous determination of anisotropic residual stresses and texture by x-ray diffraction, Journal of Applied Physics 76 (1994) 7246.
[28] L. Nie, Z. Liu, M. Liu, L. Yang, Y. Zhang, Enhanced performance of $La_{0.6}Sr_{0.4}Co_{0.2}Fe_{0.8}O_{3-\delta}$ (LSCF) cathodes with graded microstructure fabricated by tape casting, Journal of The Electrochemical Science and Technology 1 (2010) 50–56.
[29] M.B. Suresh, T.H. Yeh, C.C. Chou, Zn doped LSCF as a novel cathode material for solid oxide fuel cell, Integrated Ferroelectrics, International Journal 121 (2010) 113.
[30] A. Ghosh, A.K. Sahu, A.K. Gulnar, A.K. Suri, Synthesis and characterization of lanthanum strontium manganite, Scripta Materialia 52 (2005) 1305.
[31] W. Zhou, Z.P. Shao, R. Ran, H.X. Gu, W. Jin, N. Xu, LSCF nanopowder from cellulose–glycine–nitrate process and its application in intermediate-temperature solid oxide fuel cells, Journal of the American Ceramic Society 91 (2008) 1155–1162.
[32] M. Ghouse, Y. Al-Yousef, A. Al-Musa, M.F. Al-Otaibi, Preparation of $La_{0.6}Sr_{0.4}Co_{0.2}Fe_{0.8}O_3$ nanoceramic cathode powders for solid oxide fuel cell (SOFC) application, International Journal of Hydrogen Energy 35 (2010) 9411–9419.
[33] R.A. Vargas, R. Chiba, M. Andreoli, E.S.M. Seo, Síntese e caracterização de $La_{1-x}Sr_xMnO_{3\pm\delta}$ e $La_{1-x}Sr_xCo_{1-y}Fe_yO_{3-\delta}$ utilizados como catodo em células a combustível de óxido sólido, Cerâmica 54 (2008) 366–372.
[34] J.M. Vohs, R.J. Gorte, High-performance SOFC cathodes prepared by infiltration, Advanced Materials 21 (2009) 943–956.
[35] F. Zhao, A.V. Virkar, Dependence of polarization in anode-supported solid oxide fuel cells on various cell parameters, Journal of Power Sources 141 (2005) 79–95.
[36] V.V. Kharton, E.N. Naumovich, A.A. Vecher, Research on the electrochemistry of oxygen ion conductors in the former Soviet Union. I. ZrO_2-based ceramic materials, Journal of Solid State Electrochemistry 3 (1999) 61.
[37] S.B. Adler, J.A. Lane, B.C.H. Steele, Electrode kinetics of porous mixed-conducting oxygen electrodes, Journal of the Electrochemical Society 143 (1996) 3554.
[38] X.J. Chen, S.H. Chan, K.A. Khor, Simulation of a composite cathode in solid oxide fuel cells, Electrochimica Acta 49 (2004) 1851.
[39] J. Choi, J. Im, I. Park, D. Shin, Preparation and characteristics of $Ba_{0.5}Sr_{0.5}Co_{0.8}Fe_{0.2}O_{3-\delta}$ cathodes for IT-SOFCs by electrostatic slurry spray deposition, Ceramics International 38 (2012) S489–S492.